Rocksalt CeO epitaxial thin film as a heavy-fermion system transiting from math xmlns="http://www.w3.org/1998/Math/MathML">mi>p/mi> /math>-type metal to partially compensated math xmlns="http://www.w3.org/1998/Math/MathML">mi>n/mi> /math>-type metal by math xmlns="http://www.w3.org/1998/Math/MathML">mrow>mn >4/mn>mi>f/mi>/mrow>/math> delocalization

Nobuto Abe, Daichi Oka, Kenichi Kaminaga, Daisuke Shiga, Daichi Saito, Taku Yamamoto, Noriaki Kimura, Hiroshi Kumigashira, and Tomoteru Fukumura

Phys. Rev. B **106**, 125106 — Published 6 September 2022

DOI: 10.1103/PhysRevB.106.125106

Rock-salt CeO epitaxial thin film as a heavy fermion system transiting from p-type metal to partially compensated n-type metal by 4f delocalization

Nobuto Abe,[1] Daichi Oka,[1] Kenichi Kaminaga,[2,3] Daisuke Shiga,[4] Daichi Saito,[1] Taku Yamamoto,[1] Noriaki Kimura,[5] Hiroshi Kumigashira,[4,6] and Tomoteru Fukumura[1,2,7,8]

[1] Department of Chemistry, Graduate School of Science, Tohoku University, Sendai 980-8578, Japan

[2] Advanced Institute for Materials Research (WPI-AIMR) and Core Research Cluster, Tohoku University, Sendai 980-8577, Japan

[3] Department of Applied Chemistry, School of Engineering, Tohoku University, Sendai 980-8579, Japan

[4] Institute of Multidisciplinary Research for Advanced Materials (IMRAM), Tohoku University, Sendai 980–8577, Japan

[5] Department of Physics, Graduate School of Science, Center for Low Temperature Science, Tohoku University, Sendai 980-8578, Japan

[6] Photon Factory, Institute of Materials Structure Science, High Energy Accelerator Research Organization (KEK), Tsukuba 305–0801, Japan

[7] Center for Science and Innovation in Spintronics, Organization for Advanced Studies, Tohoku University, Sendai 980-8577, Japan

[8] Center for Spintronics Research Network, Tohoku University, Sendai 980-8577, Japan

Abstract

Rock-salt CeO (001) epitaxial thin films were synthesized and their electronic properties were

investigated. A simple $4f^1 5d^1$ electronic configuration with 4f-5d hybridization in CeO was confirmed by x-ray photoemission and absorption spectroscopy. While 5d conduction holes governed the metallic conduction at high temperatures, a partially compensated n-type conduction appeared below ~10 K with a rapid decrease in resistivity corresponding to Fermi liquid state. The hole mobility was as high as 646 $cm^2V^{-1}s^{-1}$ at 2 K in contrast to the two decades lower electron mobility, reflecting the large and small dispersion of 5d and 4f bands, respectively. At 0.8 K, a resistivity minimum was observed as a manifestation of the Kondo effect, indicating partial 4f localization. These results represented that the significant 4f-5d hybridization induced a Kondo coherent state in CeO with a short Ce-Ce interionic distance unlike the other antiferromagnetic Ce chalcogenides.

INTRODUCTION

Intermetallic Ce compounds have been widely studied as a heavy fermion system containing significantly hybridized 4f and conduction electrons [1–3], generating fascinating electronic and magnetic phenomena such as extremely large effective charge-carrier mass in $Ce(Cu,Au)_6$ [4], multiple metamagnetic transitions in Ce monopnictides [5,6], heavy fermion superconductivity in $CeCu_2Si_2$ [7], and energy gap formation via Kondo effect in $Ce_3Bi_4Pt_3$ [8]. Those rich electronic and magnetic phases generally reside in the Doniach phase diagram as a function of hybridization between the conduction and 4f electrons [9,10]. Strong hybridization makes the Kondo coupling dominating over the Ruderman–Kittel–Kasuya–Yosida interaction, stimulating itinerancy of 4f electrons at low temperatures.

So far, temperature-induced reconstruction of the Fermi surface in heavy fermion systems has been intensively studied by various experimental techniques [11–13]. The Hall effect measurements have not been useful to evaluate quantitatively the amounts of charge carriers associated with the 4f delocalization, because of the intricate Hall signals due to large anomalous Hall effect and/or multiple band carriers [14,15]. Rock-salt type Ce monochalcogenides Ce*Ch*s (*Ch* = O, S, Se, and Te) possess simple $5d^14f^1$ electronic configurations, thus are suitable to investigate heavy fermion phenomena via electrical measurements. For *Ch* = S, Se, and Te, the 5d conduction electrons contribute to the metallic conduction with local resistivity minima due to the Kondo effect, followed by the resistivity drop associated with antiferromagnetic phase transition at lower temperatures [16]. The higher antiferromagnetic phase transition temperature for smaller anion in Ce*Ch* [CeS (8.4 K), CeSe (5.6 K), and CeTe (2.2 K) (ref. 17)], indicates that Ce*Ch* with smaller anion is closer to the quantum critical point. This chemical trend can be a consequence of larger 4f-5d transfer integral and closer energy between the 4f and 5d bands for the smaller *Ch* anions [18], as seen in Ce monopnictides [19]. According to the Doniach phase diagram, Kondo coherent states

dominate over the antiferromagnetism by applying external pressure in Ce*Ch* [16]. Therefore, the much smaller lattice constant of CeO (5.089 Å) than those of CeS (5.778 Å), CeSe (5.992 Å), and CeTe (6.36 Å) [17,20] would show a heavy fermion state under the strongest 4f-5d hybridization. Indeed, a theoretical calculation predicted a semimetallic band structure, where the 5d and 4f bands formed hole and electron pockets around the Fermi level, respectively [21], suggesting the high hole mobility that is rare for oxides. However, CeO has not been synthesized for 40 years without investigation of its physical properties due to the difficulty in synthesizing CeO with an unusual charge state of Ce^{2+} [20,22].

Recently, metastable rock-salt rare-earth monoxides have been synthesized for various rare-earth elements such as Y, La, Pr, Nd, Sm, Gd, Ho, Yb, and Lu by using pulsed laser deposition [23–31]. In this study, we synthesized CeO epitaxial thin films and investigated their physical properties. CeO epitaxial thin films were paramagnetic metal and showed a Fermi-liquid behavior below ~10 K, where a transition from p-type metal to partially compensated n-type metal was induced by 4f delocalization. With further decreasing temperature down to 0.2 K, Kondo effect was observed, indicating that small portion of 4f electrons remained localized even at such low temperatures.

EXPERIMENT

CeO epitaxial thin films were synthesized on $YAlO_3$ (110) substrates at 250 °C by pulsed laser deposition. A Ce metal (99.9%) target was irradiated by KrF excimer laser (λ = 248nm) with laser energy of 1.0 J/cm^2 and repetition rate of 10 Hz in an ultrahigh vacuum chamber with base pressure of ~6×10^{-9} Torr. Pure O_2 gas was supplied during the film synthesis with the partial pressure of 2.4×10^{-8} Torr, monitored by a quadrupole mass spectrometer. The typical film thickness measured by x-ray reflection was about 6 nm. In order to prevent the film degradation, an amorphous AlO_x insulating layer (~6 nm thick) was *in situ* deposited on the

film at room temperature. Crystal structure was characterized by x-ray diffraction (XRD) with a four-axis diffractometer (D8 Discover, Bruker AXS). Hard x-ray photoelectron spectroscopy (HAXPES) was performed using an incident photon energy ($h\nu$) of = 8 keV at the beamline BL47XU of the SPring-8. X-ray absorption spectroscopy (XAS) and soft x-ray photoemission spectroscopy (SXPES) were performed at the beamline BL-2A MUSASHI of the Photon Factory, KEK. All spectroscopic measurements were conducted at 300 K, and the Fermi level (E_F) was calibrated by the measurement of a gold film that was electrically connected to the sample. In the SXPES measurement, $h\nu$ was varied around Ce 3d-4f threshold for resonant photoemission measurement, where $h\nu$s of on- and off-resonance were determined by measuring XAS at Ce $M_{4,5}$ absorption edge. Electrical transport properties were evaluated for Hall-bar shaped thin films by four-probe and Hall effect measurements from 2 K to 300 K and from 0.2 K to 1.3 K using a physical property measurement system (PPMS, Quantum Design) and a dilution refrigerator (Kelvinox TLM, Oxford Instruments), respectively. Magnetic properties were measured by a magnetic property measurement system (MPMS2, Quantum Design).

RESULTS AND DISCUSSION

Figure 1(a) shows a typical XRD θ–2θ pattern of the CeO thin film on $YAlO_3$ (110) substrate. CeO 002 diffraction peak was observed without any impurity phase. The full width at half-maximum of the rocking curve around the CeO 002 peak was 0.08°, representing the high crystallinity of the thin film [inset of Fig. 1(a)]. A spot 224 diffraction peak in the two-dimensional reciprocal space map indicated coherent growth of the CeO epitaxial thin film [Fig. 1(b)]. The epitaxial relationship for the out-of-plane and in-plane directions was CeO (001) || $YAlO_3$ (110) and CeO [110] || $YAlO_3$ [001], respectively. The lattice constants of thin film were a = 5.200 Å and c = 5.150 Å, slightly larger than that of a = 5.089 Å for the bulk polycrystal

[20]. The distances between the nearest-neighbor Ce ions in the CeO thin film were 3.68 and 3.64 Å along the in-plane and out-of-plane directions, respectively, exceeding the Hill limit of 3.41 Å for Ce [32]. Accordingly, the 4f orbitals would not be directly overlapped in the CeO thin films.

In the HAXPES valence-band spectrum of the CeO thin film, the Ce 5d states were distributed within 3 eV below E_F, while the O 2p states were in the binding energies of 5–15 eV [Fig. 2(a)]. The existence of a clear Fermi edge indicated a metallic band structure of CeO with 5d conduction electrons or holes. In comparing the Ce 3d core-level spectrum of CeO taken by HAXPES with those of reference Ce metal and oxides with different oxidation states, the peak top of the $4f^1$ final-state peaks for the CeO thin film was located between those of Ce metal and Ce_2O_3 [Fig. 3(a)] [33,34], reflecting their intermediate charge state. The nature of trivalent Ce ions in metallic states for the CeO thin film were also supported by the XAS spectrum [Fig. 3(b)], where the obtained spectrum was similar to those reported for trivalent Ce intermetallic compounds [35].

To examine the 4f-5d hybridization in CeO, we next performed Ce 3d-4f resonant photoemission measurements. As shown in Fig. 2(b), the resonant spectra are reminiscent of the typical Ce intermetallic compounds [36], suggesting the substantial hybridization between 4f level and 5d conduction band. Two clear resonant enhanced peaks were observed at E_F and 3.5 eV below E_F on resonance ($h\nu$ = 882.0 eV and 882.5 eV) [Fig. 2(b)] in comparison with off-resonance ($h\nu$ = 875 eV). The sharp peak just at E_F corresponds to the so-called Kondo resonance peaks of the excitation to $4f^1$ ($4f^1 \rightarrow 4f^1\underline{c}$) final state ($\underline{c}$: a hole in the 5d conduction band), while the relatively broad peak centered around 3.5 eV is the excitation to $4f^0$ ($4f^1 \rightarrow 4f^0$) final state, respectively [37]. The former indicated itinerancy of the 4f electrons through 4f-5d hybridization, although the areal fraction of the $4f^1$ peak in total intensity of $4f^0$ + $4f^1$ peaks is small. The latter is close to the bare state of the 4f level, energetically overlapping with

the 5d states. From these results, the Ce ion in CeO was almost trivalent possessing an approximately $4f^1 5d^1$ configuration with weak but finite 4f-5d hybridization, being consistent qualitatively with the previous band calculation [21].

Figure 4(a) shows temperature T dependence of electrical resistivity ρ_{xx} for the CeO thin film from 2 K to 300 K. The ρ_{xx}–T curve during upward and downward T sweeps was reversible without any hysteresis unlike Ce metal [38], confirming no Ce metal impurity in the film. The metallic behavior ($d\rho_{xx}/dT > 0$) was consistent with the metallic band structure observed in HAXPES [Fig. 2(a)]. Below a characteristic temperature T^* of ~10 K, ρ_{xx} decreased rapidly proportional to T^2 with a coefficient A of 0.219 μΩ cm K^{-2} [inset of Fig. 4(a)], exhibiting a Fermi liquid behavior. Similar to the other heavy fermion compounds [39–41], the resistivity drop was concomitant with the sign change in magnetoresistance at 9 T from negative to positive [Fig. 4(a)]. This unconventional T dependence of ρ_{xx} is in contrast to the featureless ρ_{xx}–T curve in the normal state of superconducting LaO without 4f electron [24], indicating significant influences of the $4f^1$ electron on the electrical conduction in CeO. According to the Fermi liquid theory, $A^{-1/2}$ is proportional to the Kondo temperature T_K [42], while a relationship of $T_K \propto A^{-1/3}$ was seen in Ce-based heavy fermion compounds as well as CeO [43–50] as summarized in Fig. S1 in the Supplemental Material [51], assuming T_K = 75 K estimated for CeO from bulk modulus measurement [22]. Those results indicated that the significant 4f-5d hybridization due to the short Ce interionic distance induced not antiferromagnetism like the other Ce*Ch*s but a Kondo coherent state in CeO, as expected from the Doniach phase diagram.

With further decreasing temperature, ρ_{xx} showed a minimum around 0.8 K followed by a slight increase proportional to ln T as a manifestation of Kondo effect [Fig. 4(b)], whose origin was different from that in the above-mentioned Kondo coherent state. The possibility of weak localization was ruled out by the positive parabolic magnetoresistance even at around 25 mK as seen in Fig. S2 in the Supplemental Material [51]. Here, the ρ_{xx} can be expressed as $\rho_{xx} = \rho_r$

$+ AT^n + \rho_K$, where ρ_r is the residual resistivity, the second term is the metallic component toward the Fermi-liquid state, and ρ_K is the Kondo resistivity. The ρ_K is described by the following Hamann's equation [52],

$$\rho_K = \frac{\rho_0}{2}\left\{1 - \frac{\ln(T/T_K')}{\left[\ln^2(T/T_K') + S(S+1)\pi^2\right]^{1/2}}\right\} \quad (1)$$

where ρ_0 is the unitarity limit, T_K' is the Kondo temperature for the low-temperature Kondo scattering, and S is the spin of the magnetic impurity. The ρ_{xx}–T curve below 2.0 K was well fitted to Eq. 1 [Fig. 4(b)], yielding T_K' of 0.423 K and S of 0.087. Similar small S parameters were reported for various Ce-based Kondo compounds probably due to the crystal field effects and orbital degeneracy [53–55]. This result suggested that the Kondo effect originated from partially localized 4f electrons of Ce even in the Kondo coherent state, although we cannot fully rule out the possible contribution of the small amount of unintentional magnetic impurities.

Magnetism of the CeO thin film was investigated by magnetization measurements. The magnetization curves at 2 and 10 K did not show any hysteresis [Fig. 5(a)]. The temperature dependence of field-cooled and zero-field-cooled magnetic susceptibility almost overlapped [Fig. 5(b)], where the inversed magnetic susceptibility was proportional to temperature. Hence, the CeO thin films was paramagnetic down to 2 K. The large saturation magnetization at 2 K could be attributed to Pauli paramagnetism due to the 5d electrons, similar to the other paramagnetic Ce-based heavy fermion compounds [44,56]. The lack of magnetic ordering supported that the CeO thin film resided in the delocalization regime of the Doniach phase diagram.

Hall effect and magnetoresistance were measured at different temperatures to evaluate the carrier density and mobility [Fig. 6(a)]. At 10 K and higher, the Hall resistivity ρ_{yx} showed positively linear magnetic field dependence, indicating a simple p-type metallic conduction. The p-type character was also seen in the other Ce monochalcogenides [17]. Below 10 K, on the other hand, nonlinear magnetic field dependence of ρ_{yx} was observed, accompanied by

relatively large positive magnetoresistance [Fig. 6(b)]. This nonlinear magnetic field dependence was probably caused by presence of p-type and n-type carriers, considering the lack of magnetic ordering down to 2 K. Indeed, the magnetic field dependences of ρ_{yx} and ρ_{xx} at 2 and 5 K were well fitted by the two-carrier Drude model [the insets of Figs. 6(a) and 6(b)], validating the presence of both conduction electrons and holes.

Figure 7 shows the electron and hole carrier density and mobility as a function of temperature. At 10 K and higher, only high-density hole carriers in the order of 10^{22} cm^{-3} were present. Below 10 K, high-density conduction electrons emerged whereas the conduction holes abruptly decreased with dramatic increase of mobility up to 646 $cm^2V^{-1}s^{-1}$ at 2 K. The two-decades higher hole mobility than the electron mobility reflected the much larger dispersion of the 5d band than that of the 4f band. This electronic transition occurred at T^* = ~10 K, where ρ_{xx} showed the steep drop [Fig. 4(a)]. The electron density of 1.98×10^{22} cm^{-3} at 2 K was close to the nominal 4f electron density of 2.87×10^{22} cm^{-3} in the $4f^1$ configuration, indicating significant delocalization of 4f electrons.

Here, we discuss the possible origin of the phase transition from p-type metal to partially compensated n-type metal in the CeO thin film. At high temperatures above T^*, the 4f electrons were fully localized because of the weak 4f-5d hybridization as observed by SXPES. Thus, the 5d conduction holes dominated the electrical conduction, which is qualitatively consistent with the calculated band structure with a large hole pocket [21]. With decreasing temperature down to T^*, the enhanced hybridization would open a gap state in the 5d band [57], leading to the significant decrease in the 5d conduction holes. At the same time, majority of the 4f electrons delocalized as described above. The slightly lower carrier density than the nominal 4f electron density also indicated that a small fraction of 4f electrons remained localized even below T^*, which could induce the Kondo effect at such low temperatures [Fig. 4(b)].

CONCLUSION

CeO (001) epitaxial thin films on $YAlO_3$ (110) substrates were synthesized by PLD. X-ray photoemission and absorption spectroscopy indicated $4f^1 5d^1$ electronic configuration with relatively weak 4f-5d hybridization. The CeO thin film showed p-type metallic conduction at high temperatures and phase transition to partially compensated n-type metal with a Fermi liquid behavior at T^* = ~10 K. The electrical conduction below T^* was well explained by the two-carrier Drude model reflecting the simple electronic configuration of CeO. The high (low) carrier density and low (high) mobility of conduction electrons (holes) suggested gap formation in the 5d band due to the 4f-5d hybridization at T^*. At significantly lower temperature than T^*, Kondo effect was probably caused by the small fraction of 4f electrons remaining localized. Further investigations such as low temperature photoemission spectroscopy would elucidate the band structure associated with the transition from p-type metal to partially compensated n-type metal in CeO.

ACKNOWLEDGMENTS

This work was financially supported by Grants-in-Aid for Scientific Research (Nos. 18H03872, 18K18935, 19K15440, 19F19347, 20H02704, and 21H05008) from the Japan Society for the Promotion of Science (JSPS), and CREST (JPMJCR18T1) from the Japan Science and Technology Agency (JST). The hard x-ray photoemission measurements at SPring-8 were conducted under approval of the Japan Synchrotron Radiation Research Institute (2019B1248). The work performed at KEK-PF was approved by the Program Advisory Committee (proposals 2018S2-004 and 2021S2-002) at the Institute of Materials Structure Science, KEK.

References

[1] G. R. Stewart, Rev. Mod. Phys. **56**, 755 (1984).

[2] P. Coleman, C. Pépin, Q. Si, and R. Ramazashvili, J. Phys. Condens. Matter **13**, R723 (2001).

[3] P. Gegenwart, Q. Si, and F. Steglich, Nat. Phys. **4**, 186 (2008).

[4] A. Schröder, G. Aeppli, R. Coldea, M. Adams, O. Stockert, H. V. Löhneysen, E. Bucher, R. Ramazashvili, and P. Coleman, Nature **407**, 351 (2000).

[5] T. Inoue, T. Kuroda, K. Sugiyama, Y. Haga, T. Suzuki, and M. Date, J. Phys. Soc. Jpn. **64**, 572 (1995).

[6] J. Rossat-Mignod, P. Burlet, S. Quezel, J. M. Effantin, D. Delacôte, H. Bartholin, O. Vogt, and D. Ravot, J. Magn. Magn. Mater. **31–34**, 398 (1983).

[7] F. Steglich, J. Aarts, C. D. Bredl, W. Lieke, D. Meschede, W. Franz, and H. Schäfer, Phys. Rev. Lett. **43**, 1892 (1979).

[8] M. F. Hundley, P. C. Canfield, J. D. Thompson, Z. Fisk, and J. M. Lawrence, Phys. Rev. B **42**, 6842 (1990).

[9] S. Doniach, Physica B+C **91**, 231 (1977).

[10] S. Hoshino and Y. Kuramoto, Phys. Rev. Lett. **111**, 026401 (2013).

[11] P. T. Coleridge, J. Phys. F: Met. Phys. **17**, L79 (1987).

[12] S. K. Goh, J. Paglione, M. Sutherland, E. C. T. O'farrell, C. Bergemann, T. A. Sayles, and M. B. Maple, Phys. Rev. Lett. **101**, 056402 (2008).

[13] S. Jang, J. D. Denlinger, J. W. Allen, V. S. Zapf, M. B. Maple, J. N. Kim, B. G. Jang, and J. H. Shim, Proc. Natl. Acad. Sci. **117**, 23467 (2017).

[14] S. Nair, S. Wirth, S. Friedemann, F. Steglich, Q. Si, and A. J. Schofield, Adv. Phys. **61**, 583 (2012).

[15] K. Winzer, Z. Phys. B Condens. Matter **64**, 159 (1986).

[16] Y. Hayashi, S. Takai, T. Matsumura, H. Tanida, M. Sera, K. Matsubayashi, Y. Uwatoko,

and A. Ochiai, J. Phys. Soc. Jpn. **85**, 034704 (2016).

[17] F. Hulliger, B. Natterer, and H. R. Ott, J. Magn. Magn. Mater. **8**, 87 (1978).

[18] M. Nakayama, H. Aoki, A. Ochiai, T. Ito, H. Kumigashira, T. Takahashi, and H. Harima, Phys. Rev. B **69**, 155116 (2004).

[19] A. Fujimori and J. H. Weaver, Phys. Rev. B **31**, 6345 (1985).

[20] J. M. Leger, N. Yacoubi, and J. Loriers, J. Solid State Chem. **36**, 261 (1981).

[21] S. K. De and S. Chatterjee, J. Phys. Condens. Matter **1**, 1169 (1989).

[22] J. M. Léger, Physica B **190**, 84 (1993).

[23] K. Kaminaga, R. Sei, K. Hayashi, N. Happo, H. Tajiri, D. Oka, T. Fukumura, and T. Hasegawa, Appl. Phys. Lett. **108**, 122102 (2016).

[24] K. Kaminaga, D. Oka, T. Hasegawa, and T. Fukumura, J. Am. Chem. Soc. **140**, 6754 (2018).

[25] H. Shimizu, D. Oka, K. Kaminaga, D. Saito, T. Yamamoto, N. Abe, N. Kimura, D. Shiga, H. Kumigashira, and T. Fukumura, Phys. Rev. B **105**, 014442 (2022).

[26] D. Saito, K. Kaminaga, D. Oka, and T. Fukumura, Phys. Rev. Mater. **3**, 064407 (2019).

[27] Y. Uchida, K. Kaminaga, T. Fukumura, and T. Hasegawa, Phys. Rev. B **95**, 125111 (2017).

[28] T. Yamamoto, K. Kaminaga, D. Saito, D. Oka, and T. Fukumura, Appl. Phys. Lett. **117**, 052402 (2020).

[29] T. Amrillah, D. Oka, H. Shimizu, S. Sasaki, D. Saito, K. Kaminaga, and T. Fukumura, Appl. Phys. Lett. **120**, 082403 (2022).

[30] T. Yamamoto, K. Kaminaga, D. Saito, D. Oka, and T. Fukumura, Appl. Phys. Lett. **114**, 162104 (2019).

[31] K. Kaminaga, D. Oka, T. Hasegawa, and T. Fukumura, ACS Omega **3**, 12501 (2018).

[32] J. Tang and K. A. Gschneidner, J. Less Common Met. **149**, 341 (1989).

[33] R. Eloirdi, P. Cakir, F. Huber, A. Seibert, R. Konings, and T. Gouder, Appl. Surf. Sci. **457**, 566 (2018).

[34] E. Wuilloud, H. R. Moser, W.-D. Schneider, and Y. Baer, Phys. Rev. B **28**, 7354 (1983).

[35] L. Howald, E. Stilp, P. D. de Réotier, A. Yaouanc, S. Raymond, C. Piamonteze, G. Lapertot, C. Baines, and H. Keller, Sci. Rep. **5**, 12528 (2015).

[36] E. Weschke, C. Laubschat, T. Simmons, M. Domke, O. Strebel, and G. Kaindl, Phys. Rev. B **44**, 8304 (1991).

[37] O. Gunnarsson and K. Schönhammer, Phys. Rev. B **28**, 4315 (1983).

[38] P. Burgardt, K. A. Gschneidner, D. C. Koskenmaki, D. K. Finnemore, J. O. Moorman, S. Legvold, C. Stassis, and T. A. Vyrostek, Phys. Rev. B **14**, 2995 (1976).

[39] G. Remenyi, A. Briggs, J. Flouquet, O. Laborde, and F. Lapierre, J. Magn. Magn. Mater. **31–34**, 407 (1983).

[40] A. Sumiyama, Y. Oda, H. Nagano, Y. Ōnuki, K. Shibutani, and T. Komatsubara, J. Phys. Soc. Jpn. **55**, 1294 (1986).

[41] N. Kawakami and A. Okiji, J. Phys. Soc. Jpn. **55**, 2114 (1986).

[42] S. Raymond and D. Jaccard, J. Low Temp. Phys. **120**, 107 (2000).

[43] H. R. Ott, H. Rudigier, Z. Fisk, J. O. Willis, and G. R. Stewart, Solid State Commun. **53**, 235 (1985).

[44] H. G. Schlager, A. Schröder, M. Welsch, and H. v. Löhneysen, J. Low Temp. Phys. **90**, 181 (1993).

[45] P. Haen, J. Flouquet, F. Lapierre, P. Lejay, and G. Remenyi, J. Low Temp. Phys. **67**, 391 (1987).

[46] M. J. Besnus, J. P. Kappler, P. Lehmann, and A. Meyer, Solid State Commun. **55**, 779 (1985).

[47] D. Gignoux, F. Givord, R. Lemaire, and F. Tasset, J. Less Common Met. **94**, 165 (1983).

[48] Y. Ōnuki, T. Yamazaki, T. Omi, I. Ukon, A. Kobori, and T. Komatsubara, J. Phys. Soc. Japan **58**, 2126 (1989).

[49] J. D. Thompson, J. M. Lawrence, and Z. Fisk, J. Low Temp. Phys. **95**, 59 (1994).

[50] I. Umehara, Y. Kurosawa, N. Nagai, M. Kikuchi, K. Satoh, and Y. Ōnuki, J. Phys. Soc. Japan **59**, 2848 (1990).

[51] See Supplemental Material at [URL will be inserted by publisher] for A vs. T_K for various Ce-based paramagnetic Kondo compounds, and magnetoresistance below 2 K for CeO epitaxial thin film.

[52] D. R. Hamann, Phys. Rev. **158**, 570 (1967).

[53] M. Dietrich, W. Gey, and E. Umlauf, Solid State Commun. **11**, 655 (1972).

[54] K. Winzer, Solid State Commun. **16**, 521 (1975).

[55] T. Komatsubara, N. Sato, S. Kunii, I. Oguro, Y. Furukawa, Y. Onuki, and T. Kasuya, J. Magn. Magn. Mater. **31**–**34**, 368 (1983).

[56] Y. Ōnuki, Y. Shimizu, and T. Komatsubara, J. Phys. Soc. Jpn. **54**, 304 (1985).

[57] S. Pal, C. Wetli, F. Zamani, O. Stockert, H. V. Löhneysen, M. Fiebig, and J. Kroha, Phys. Rev. Lett. **122**, 096401 (2019).

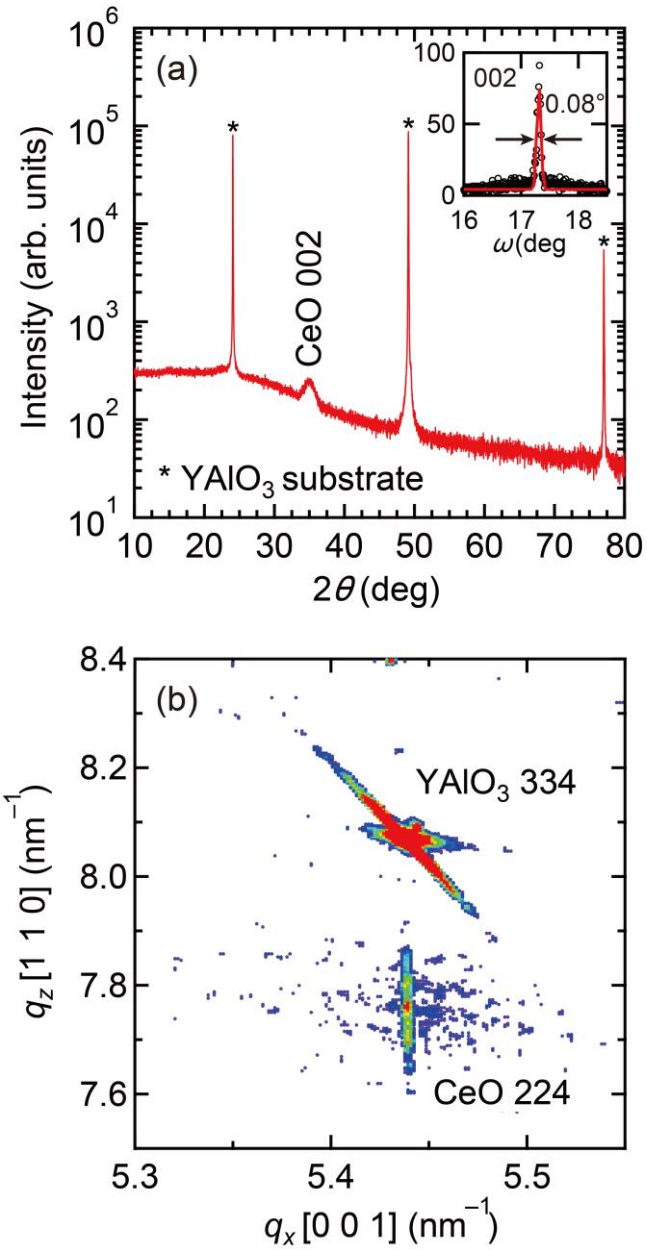

FIG. 1. (a) XRD θ–2θ pattern for CeO epitaxial thin film on $YAlO_3$ (110) substrate. Inset shows rocking curve around the CeO 002 diffraction. (b) Reciprocal space map around 224 diffraction for the CeO epitaxial thin film.

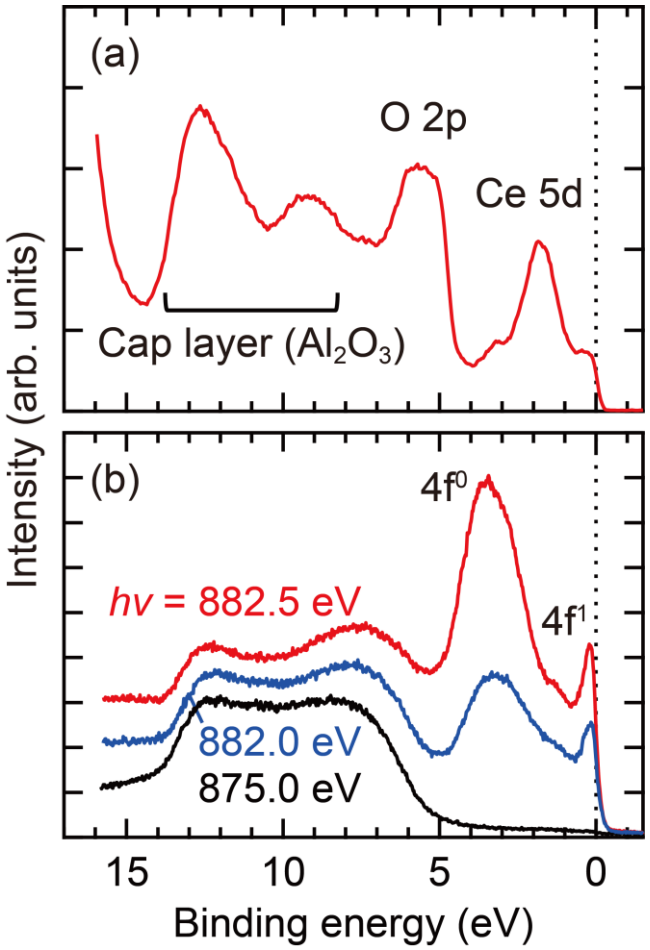

FIG. 2. Valence band photoemission spectra for an AlO_x-capped CeO epitaxial thin film taken by (a) HAXPES at $h\nu = 8$ keV and (b) SXPES at the energies around the Ce M-edge absorption edge. Because amorphous AlO_x is an insulator with a band gap of more than 6 eV, an AlO_x capping layer does not mask the electronic structures in the energy range from $E_F - 5$ eV to E_F derived from the Ce 5d and 4f states of the buried CeO film [25].

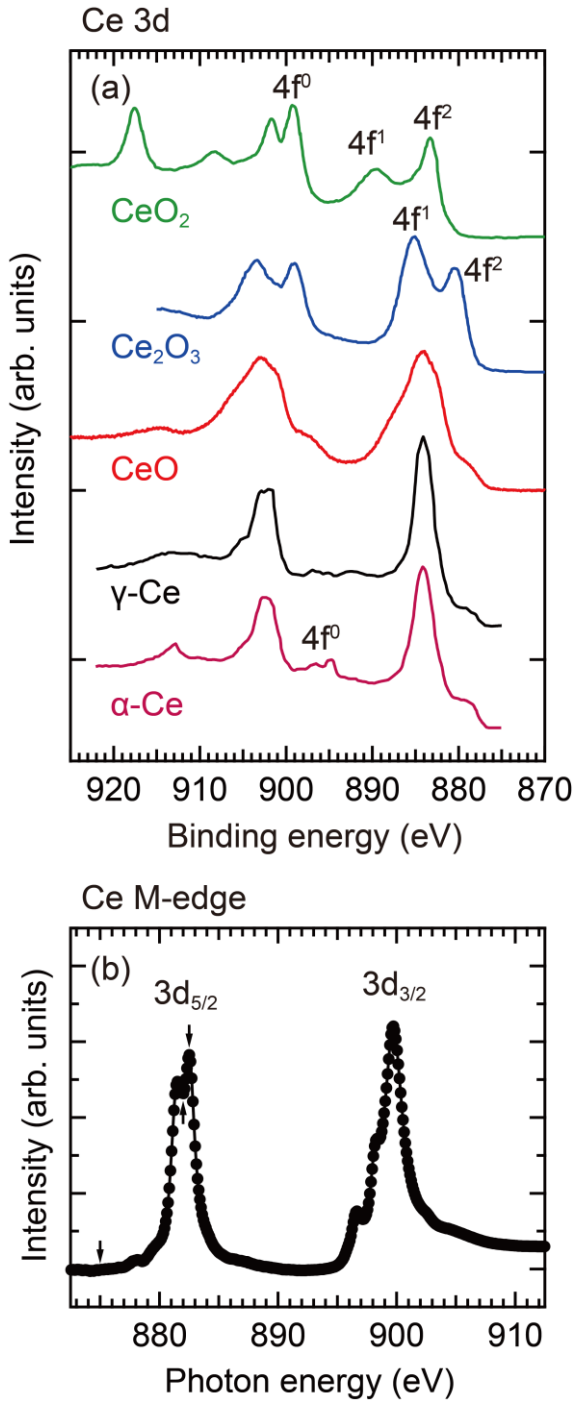

FIG. 3. (a) Ce 3d core-level spectrum obtained by hard x-ray photoemission and (b) x-ray absorption spectrum at Ce M-edge for CeO epitaxial thin film. Spectra for α-Ce, γ-Ce, Ce_2O_3 and CeO_2 are shown in (a) as references [33, 34]. The arrows in (b) denote the energies used in the on- and off-resonant soft X-ray photoemission spectroscopy in Fig. 2(b).

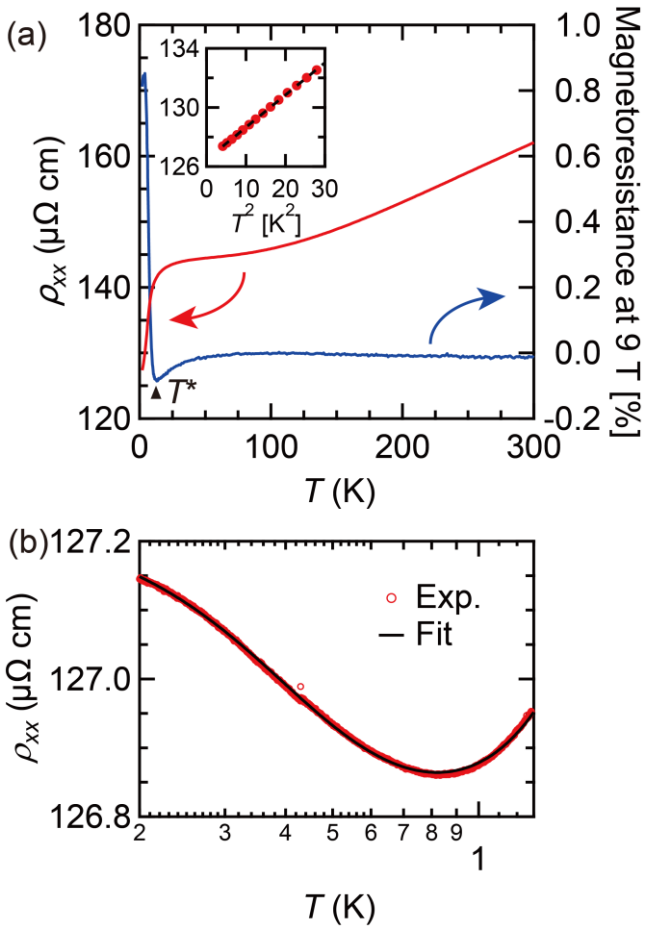

FIG. 4. (a) T dependence of ρ_{xx} and magnetoresistance at 9 T from 2 K to 300 K for CeO epitaxial thin film. Inverse triangle denotes T*. Inset shows ρ_{xx} as a function of T^2 from 2 K to 9 K. Dotted line is a linear fit. (b) T dependence of ρ_{xx} from 0.2 to 1.3 K for CeO epitaxial thin film. Fitting result with Eq. (1) is also shown (black curve).

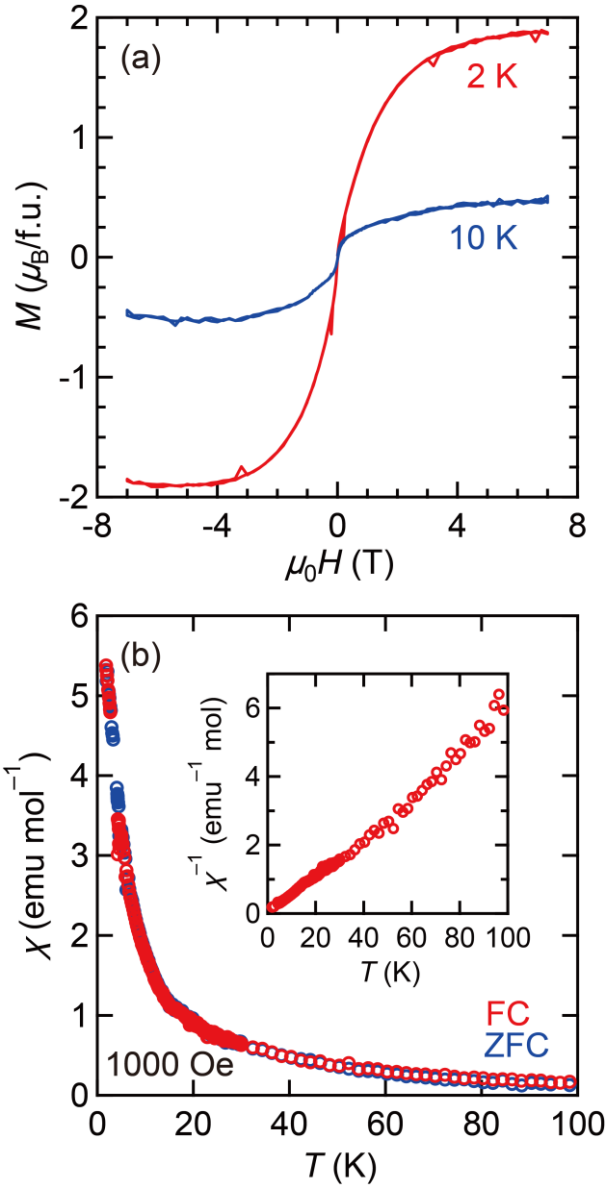

FIG. 5. (a) Magnetization curves at 2 K and 10 K and (b) temperature dependence of magnetic susceptibility under field-cooled and zero-field-cooled conditions for CeO epitaxial thin film. Inset in (b) shows inversed magnetic susceptibility as a function of temperature. The magnetic field was applied along in-plane direction.

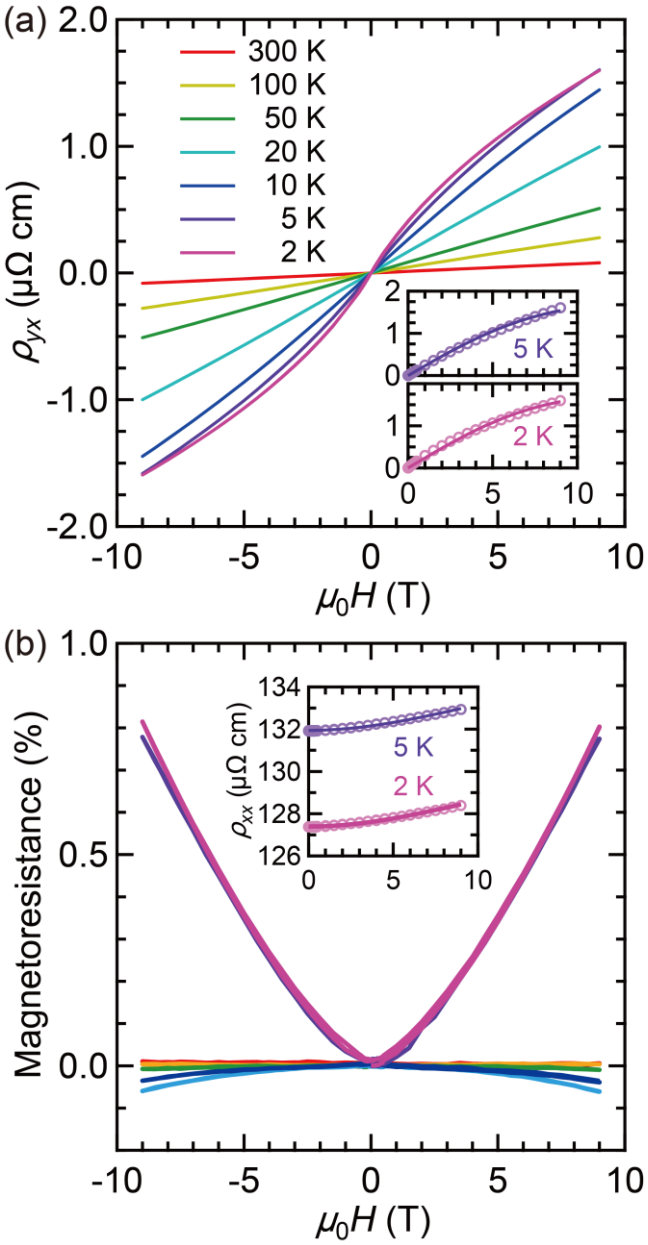

FIG. 6. Magnetic field dependence of (a) Hall resistivity and (b) magnetoresistance for CeO epitaxial thin film. Insets of (a) and (b) show the fitting results (solid lines) by the two-carrier Drude model.

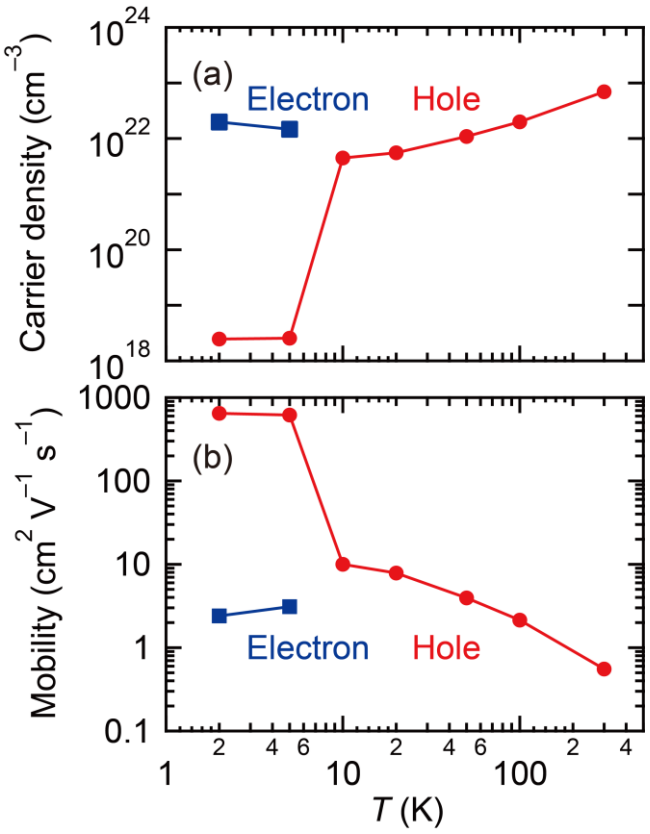

FIG. 7. *T* dependence of (a) electron (square) and hole (circle) carrier density and (b) mobility for CeO epitaxial thin film.